Dynamic model of isothermal moving bed reducer for chemical looping hydrogen production

Priyam **Kataria,** ***Wan Sieng*** **Yeo*** **and** ***Jobrun*** **Nandong**

Department of Chemical and Energy Engineering, Curtin University Malaysia, CDT 250, 98009 Miri, Sarawak, Malaysia

*christineyeo@curtin.edu.my

Abstract. This paper investigates process modelling and reactor design for the reducer in the chemical looping hydrogen production (CLHP) process. The CLHP process adopts a three-reactor technology that can provide an efficient and sustainable alternative to the current hydrogen production technology via steam methane reforming (SMR), which suffers from several limitations during industrial operation. CLHP can achieve higher thermal efficiency than SMR and provide a carbon capture and storage (CCS) system. So far, no report on the modelling analysis of the reducer despite its critical dependence on temperature. The modelling study adopts the modified pellet-grain model at the micro-scale and counter-current moving bed model reactor at the reactor level. Simulation results of the gas-solid behavior based on the multi-scale model agree with the literature evidence. Critical information from the model revealed that the oxygen carriers (solids) can attain a desired state, but the syngas remains underutilized. The model simulation further suggests that lowering the gas-solid velocity ratio (Vgs) can substantially promote the syngas conversion. However, the Vgs value must remain above a threshold value (170), defined through the limitation of gas-solid velocities in a moving bed reactor. Since a CCS system requires high purity (>95%) of the product gas, rigorous temperature-pellet size optimization is vital to achieving the target purity while maintaining desired solid state.

1. Introduction

Energy demand over the previous decades has grown exponentially leading to increased utilization of non-renewable fossil fuels, which release carbon dioxide (CO_2) upon combustion. The energy industry remains the largest contributor to greenhouse gas (GHG) emissions, raising major concerns over global warming [1]. Therefore, a significant portion of research has been dedicated to producing sustainable alternatives with low environmental impact. Hydrogen (H_2) is one such alternative, demonstrating excellent combustion efficiency in fuel cells and releasing only water steam (H_2O) as a by-product. It is highlighted in several literatures as a promising fuel with the capability to completely substitute the existing non-renewable sources [2]. The hesitation towards the adoption of H_2 arises from its high prices compared to fossil fuels, presenting a crucial challenge for producing affordable H_2 [3].

Chemical looping hydrogen production (CLHP) is a novel technology of H_2 production presenting physical and thermodynamic advantages, with efficient recovery pathways. CLHP also offers attractive carbon capture and storage (CCS) strategy implementation, which can avoid major capital

and operating costs for purification [4]. Therefore, this CLHP process is considered suitable for industrial H_2 production and substitutes for the existing methods that have inefficiency. Some previous investigations on the CLHP process have targeted developing such simulations, verifying the mathematically formulated kinetics from bench-scale experiments [5, 6]. However, the research on this CLHP topic is highly limited and restricted to bench-scale analyses [7]. Despite its promising experimental results, the CLHP process modelling and reactor design are still minimal in the literature. Hence, dynamic models for CLHP are essential components for testing the applicability of under realistic constraints.

On the other hand, Kataria, Nandong [8] had reviewed several design and control aspects of the closed-loop reactor system, identifying suitable reactants, operating modes, and computational modelling procedures. However, very limited of the reviewed research has attempted to assess any criteria involving process optimization and scale-up assessment of this CLHP technology. Therefore, the identification of large-scale limitations is essential to devise appropriate control strategies, which can be achieved through rigorous testing of system dynamics. To address this limitation, this study attempts to develop an isothermal dynamic model of the CLHP reducer, representing the first unit in the three-reactor chemical loop. Relevant information regarding the expected process behavior and operation type was presented through a detailed review of the literature. Then, utilizing the essential information, gas-solid concentration profiles were derived at both pellet and reactor scales using the modified grain model (MGM). Moreover, systematic deviations from the literature (non-isothermal) were justified through the selected operating conditions such as temperature, pressure, and the molar ratio of syngas components. The formulated system was then evaluated under the effect of changing gas-solid flow rates, to promote gas conversion. Strategies for further optimization were discussed, along with scale-up restrictions which may limit the output performance. The findings serve as a contribution towards the commercial applications of this technology, which may be vital for generating affordable H_2 at an industrial scale.

2. Chemical looping hydrogen production

The first paragraph after a heading is not indented (Bodytext style). The theoretical concept of CLHP originated from a technology known as chemical looping combustion (CLC), employing solid particles for fuel combustion. Between the late 19^{th} to early 20^{th} century, CLC principles were utilized to produce a variety of industrial gases, including CO_2, carbon monoxide (CO), syngas, and oxygen (O_2). Richter and Knoche [9] proved the inherent thermal superiority of the CLC process due to its reversibility, lowering the system entropy and displaying high exergy (available energy) efficiency. Owing to these advantages, recent literature has abundant investigations of the CLC technology as an effective CCS strategy in the energy industry [10].

The typical CLC scheme consists of a two-reactor loop circulating a solid oxygen carrier (OC), that reacts with multiple gases. Reduction of OC is carried out in the reducer, where a hydrocarbon fuel is converted to a CO_2 and H_2O mixture. The O_2-deficient solid is then circulated to the combustor, where a reaction with process air (nitrogen and O_2) regenerates the OC to its original state [11]. This typical CLC configuration was utilized to produce limited quantities of H_2 fuel for key industries in the early 1900s, primarily due to low output. Eventually in the 1930s, SMR overtook this approach as the SMR could demonstrate a higher conversion (up to 75%). But, the SMR process is expensive and inefficient from a thermodynamic perspective, along with increased production cost (up to 22%) through the addition of CCS systems can increase production costs by up to 22%, leading to high prices of H_2 compared to fossil fuels [12]. Consequently, the high fuel prices drive the majority of the H_2 productions towards non-renewable resources [12]. Alternative renewable techniques such as biomass gasification and dark fermentation can lower the H_2 production costs, although low yields incur optimization challenges [13, 14]. Moreover, high-efficiency water-splitting (electrolysis/thermolysis) strategies for the H_2 production require extreme operating conditions [15, 16]. Thus, it is crucial to develop economic and renewable solutions for achieving sustainable substitution of fossil fuels, especially in nations struggling with energy affordability [17].

2.1. Reactor system description

Chiesa, Lozza [18] proposed a novel CLC configuration including an additional reactor called oxidizer, proposing it as a critical modification for addressing efficiency concerns. Solids exiting the reducer undergo partial oxidation through steam (H_2O) producing H_2/H_2O in the oxidizer's gas outlet. The combustor returns the solid OC to its original state, thus closing the chemical loop. Multiple heat and product recovery strategies were identified, highlighting the industrial relevance of employing this new approach. This three-reactor CLHP system has been investigated in various literatures since, although the analysis remains primarily theoretical [19].

The process demonstrated in Fig. 1 describes a CLHP scheme circulating iron oxide OC, reduced by syngas fuel. The majority of existing research in CLC employs methane-based fuel reduction since natural gas is a common fuel [20]. Substitution of non-renewable sources is essential, and research focus is increasing towards adopting renewable biofuels such as syngas. Biomass has been considered a suitable source for producing syngas due to abundant availability and favorable gasification pathways [21-23]. OC serves as the key reactant in any CLC system due to its continuous cyclic movement, affecting all reactor conversions. Kang, Kim [24] investigated the performance of 16 potential OCs, evaluated based on several criteria relating to physical stability, reaction feasibility, and redox selectivity. The iron-based OCs are the most appropriate alternative for large-scale syngas production, as they display high gas conversions, adequate mechanical properties, and cost-effectiveness [25].

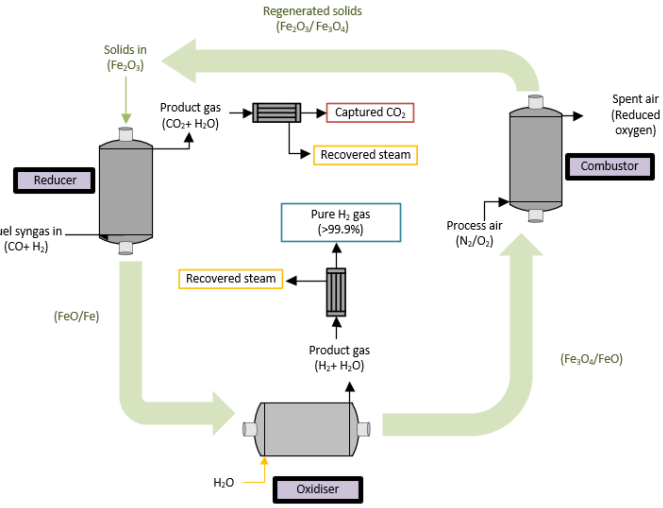

Fig. 1. Schematic for CLHP reactor system [8]

In conjunction with the selected materials for CLHP reactor system, the schematic in Fig. 1 offers several physical and thermodynamic advantages. Completely converted syngas exiting the reducer can utilize a condenser to separate pure CO_2 from H_2O, resulting in an economically efficient CCS approach [4]. Pure H_2 gas is generated in the oxidizer through the steam-iron process, avoiding significant purification expenses required for SMR. Experiments conducted with pellets including support materials observed no carbon deposition, suggesting that high-quality purification can be achieved [7, 26, 27]. The endothermic nature of fuel reduction requires an additional energy supply, identical to the SMR process. However, the exothermic reactions occurring in the combustor generate large amounts of heat, which can effectively minimize the system's energy load. Therefore, CLHP offers superior industrial performance compared to conventional methods, along with a cost-effective inherent CCS design. This CLHP technology offers tremendous potential at producing affordable H_2 fuel amid the energy crisis caused by the depletion of fossil fuels. Limited attention has been focused

on reactor design and simulation for this technology, employing primarily bench-scale models [6, 28]. No study has been found within the reviewed literature describing relevant scale-up criteria in CLHP through dynamic simulations. Hence, developing such models requires an assessment of reactor operation, serving as a basis to compute output concentrations.

2.2. Reactor type and flow regime

Chemical reactions throughout CLHP are of gas-solid nature, requiring specialized reactors vessels. Fixed-bed reactor (FBR) is the most common gas-solid reactor available within process industries. Continuous circulation cannot be achieved within FBRs, necessitating the installment of switch ports for supplying various gases into the vessel. The switching behavior in the vessel raises overpressure concerns, and advanced relief valves must be designed to ensure safe operation [29]. Heat removal is another issue in the FBR, leading to thermal sintering of the solid [30]. On the other hand, fluidized bed is another type of operation where bubbles are introduced in the packed solids through high gas flow rates. This fluidized bed generates a non-stationary behavior, leading to improved conversions and thermal efficiency. The bubbling action leads to the presence of dust in the gas stream, and product separation equipment such as cyclones is essential [31]. Moreover, the near-perfect mixing of gases in the fluidized bed can lead to a large vessel size for achieving desired conversions [32]. Such complexities for the fluidized bed can incur high design and operational costs, ultimately reducing the economic efficiency of the process.

Despite of that, the non-stationary solid flow can also be achieved within moving bed reactors (MBRs), where the bed is continuously circulated while contacting a gas stream. While this continuous circulation can occur in any direction, the axial flow is usually utilized to demonstrate profiles in cylindrical vessels. Besides, the countercurrent mode is typically preferred for the MBRs as it can increase the contact times within shorter lengths, providing superior economic production. Moreover, the fresh gas contacts with reduced solids and vice-versa, promoting further reactions along the increasing length. Experimental studies have confirmed the efficiency of this operation mode in CLC processes, where high conversions were achieved [33]. And, Tong, Sridhar [34] demonstrated a sub-pilot scale CLHP system operation in a countercurrent MBR. In their study, a complete (100%) carbon capture was achieved in the reducer, along with high-purity (>99.99%) H_2 gas produced through steam oxidation. In addition, no carbon deposition was detected under continuous 300-hour operation, confirming the thermodynamic advantages.

Other than that, corrosive fuel such as syngas can damage the reactor vessel from the inside, requiring expensive replacement. A suitable solution for such corrosion conditions is to adopt a multi-tubular reactor, which represents a traditional shell-and-tube heat exchanger vessel. A schematic of the reactor is illustrated in Fig. 2, with the countercurrent gas-solid flow. The reactions can be conducted within the tubes, which are easy to replace and reduce maintenance costs by a significant margin. Temperatures can be effectively controlled through the supply of heating/cooling fluid along the shell side. Moreover, the radial profiles can be ignored due to the high length-to-diameter (L/D) ratio, leading to lower modelling complexities. This configuration has been employed in the design of FBRs utilized for key commercial processes, including methanol-reforming, acetone production, and dimethyl ether synthesis [35-37]. The multi-tubular design has not been implemented for moving bed applications, although it can prove highly beneficial for CLHP process.

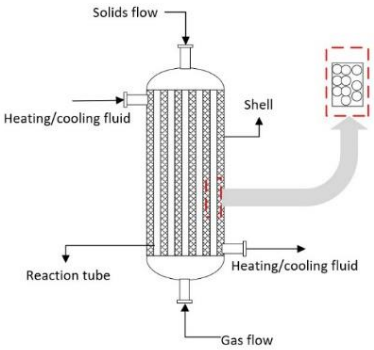

Fig. 2. Multi-tubular counter-current reactor schematic

Various details about the CLHP reactor system are discussed within this literature review section. From the existing studies, the effectiveness of the CLHP method has been proven and it demonstrates a great potential for commercial development. Apart from that, process simulations for the CLHP process using dynamic modelling are necessary for optimization and reactor scale-up evaluation. Findings from these analyses help to identify realistic constraints over the CLHP process, which serve as the basis for developing a control system. In this study, a dynamic model of the CLHP reduction was developed, assumed to be conducted in a counter-current reaction tube of tubular MBR. The computations for the CLHP reduction are adjusted to describe the isothermal operation, concerning the tube-side process optimization. The analysis can be extended to study the non-isothermal behavior controlled through heating/cooling fluid in the shell. Although the effect of temperature is explored in the current article, it represents important prospects for further research investigations.

3. Reaction modelling

The proposed reducer simulation illustrates syngas reacting with a bed of iron-oxide pellets. Modelling approach for the reducer is split into pellet and reactor scales, highlighting key derivations and initialization procedures. The developed model for the reducer can then be analyzed under varying conditions to promote necessary conversions and identify large-scale design limits.

3.1. Pellet-scale model

To represent the pellet-scale interactions, the first step is to establish a mathematical representation of the chemical reaction scheme. This chemical reactions within the reducer are identical to the direct reduction of iron (DRI), which is an established process in the steelmaking industry. Hematite (Fe_2O_3) undergoes stagewise fuel reduction to magnetite (Fe_3O_4), wüstite (FeO), and then iron ore (Fe) for complete reduction. However, in the CLHP reducer, solid conversion to FeO is deemed sufficient for steam oxidation in the oxidizer, thus reducing the amount of gas required. Meanwhile, the complete reactions must be promoted to completion, which is necessary to remove pure obtain pure CO_2 through the proposed CCS. The DRI process using syngas mixtures has also been explored within numerous literatures, and the reaction kinetic parameters as a function of temperature (T) are shown in Table 1.

Table 1. Reaction data for syngas reduced iron-oxides [38]

Reactions	k (cm/s)	$K_{eq} = \exp(a + bT + cT^{-1})$			Enthalpy at 298 K ($\Delta H_{r,298}$) (kJ/mol)
		a	b	c	
$3Fe_2O_3 + CO \underset{eqm}{\longleftrightarrow} 2Fe_3O_4 + CO_2$	$2700\exp(\frac{-113859}{RT})$	6.0259	-0.000525	5,635.3	−25.1
$Fe_3O_4 + CO \underset{eqm}{\longleftrightarrow} 3FeO + CO_2$	$25\exp(\frac{-73674}{RT})$	12.2909	-0.006183	-5,388.3	+33.6
$FeO + CO \underset{eqm}{\longleftrightarrow} Fe + CO_2$	$17\exp(\frac{-69488}{RT})$	-1.5304	-0.000729	1,610.3	−11
$3Fe_2O_3 + H_2 \underset{eqm}{\longleftrightarrow} 2Fe_3O_4 + H_2O$	$160\exp(\frac{-92092}{RT})$	6.3082	0.003788	1,822.7	−16.1
$Fe_3O_4 + H_2 \underset{eqm}{\longleftrightarrow} 3FeO + H_2O$	$23\exp(\frac{-71162}{RT})$	19.3291	-0.007725	-11,238.4	+74.8
$FeO + H_2 \underset{eqm}{\longleftrightarrow} Fe + H_2O$	$30\exp(\frac{-63627}{RT})$	0.6122	0.000362	-2,056.8	+30.2

The table above (Table 1) indicates that solid phases exist in various transition states while reacting with multiple gases. These mechanisms require mathematical models capable of illustrating the relationships among both phases. Gas-solid reaction kinetics are often established within a single pellet model integrated over the entire reactor bed. The shrinking core model (SCM) is one such mechanism, describes the reduction of the pellet core with reactions from surrounding gases. This model assumes that the gas diffuses through the solid until the surface of an unreacted core, followed by surface reactions for further shrinkage. However, experimental observations confirm the gas diffusion throughout the pellet which raises concerns regarding SCM's validity over low solid porosities [38]. The limitations of SCM can be resolved through the adoption of the grain-based model (GBM), although the computations require a higher order of complexity. GBM assumes the porous pellet to be comprised of microscopic grains undergoing a shrinking core reaction mechanism. The gas diffuses through the surface on a pellet scale, followed by reactions occurring within the grains. The concept can be further extended using MGM, to encounter multi-phase reduction under various gas mediums [38]. A conceptual description of the reducer pellet is exhibited in Fig. 3, involving both diffusion and reaction phenomena.

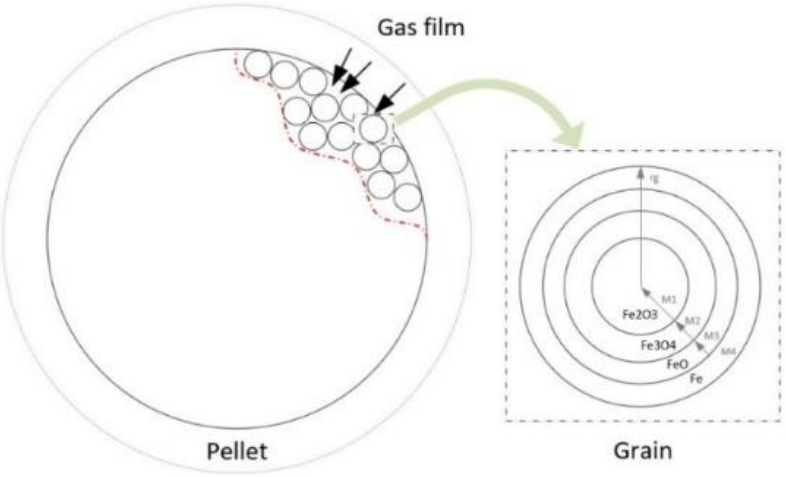

Fig. 3. Diffusion (pellet scale) and reaction (grain scale) phenomena in reduced Fe_2O_3 pellets

Prior to defining the reaction mechanisms, key model assumptions at the pellet scale that are shown in Fig. 3 are defined as follows:

P1. The pellets are spherical in shape, with symmetric grain and pore distribution.
P2. Gas from the surrounding film diffuses through the pores and then reacts through the grain surface reducing the core radius.
P3. The reduced grain volume from reactions is substituted with the product layer, thus maintaining constant pellet volume and shape.
P4. The reactions are first-order and irreversible under the defined process conditions.
P5. Resistances due to the mass transfer from the gas phase are negligible compared to outside the film transfer coefficient.
P6. Ideal gas behavior with constant volume assumption.
P7. Isothermal reaction conditions.

Assumption *P1* is employed as the symmetric design offers lower computational complexity within the proposed conceptual design [39]. The Fe_2O_3 pellet reacting within the reducer undergoes consecutive reduction, resulting in presence of multiple solid phases shown in Fig. 3. The terms *M1* (Fe_2O_3), *M2* (Fe_3O_4), *M3* (FeO), and *M4* (Fe) have been assigned to the oxidation states of the OC based on their sequence of generation. Since Fe represents the final oxidation state, the volume of phase *M4* does not reduce. In addition to stagewise solid phase change, parallel reactions from both gas species (CO and H_2) must be considered. Reduction of phase *M1* through gaseous reactants *A* (CO) and *C* (H_2) can be described using *equations 1 and 2*.

$$\alpha_{A(I)}M_1 + A \Leftrightarrow \beta_{A(I)}M_2 + \gamma_{A(I)}Q \quad \textbf{(1)}$$
$$\alpha_{C(I)}M_1 + C \Leftrightarrow \beta_{C(I)}M_2 + \gamma_{C(I)}R \quad \textbf{(2)}$$

The terms α and β in *equations 1 and 2* represent the stoichiometric coefficients of phases *M1* and *M2* respectively, within the first reduction stage. The coefficients for gaseous products *Q* (CO) and *R* (H_2) are defined through γ values in the respective equations. Each reactant phase (*M1*, *M2,* and *M3*) undergoes these parallel reactions, resulting in the total reaction set illustrated in *equation 3*.

$$\begin{array}{lll} & \textbf{Parallel} \longrightarrow & \\ \textbf{Consecutive} \downarrow & \alpha_{A(I)}M_1 + A \Leftrightarrow \beta_{A(I)}M_2 + \gamma_{A(I)}Q & \alpha_{C(I)}M_1 + C \Leftrightarrow \beta_{C(I)}M_2 + \gamma_{C(I)}R \\ & \alpha_{A(II)}M_2 + A \Leftrightarrow \beta_{A(II)}M_3 + \gamma_{A(II)}Q & \alpha_{C(II)}M_2 + C \Leftrightarrow \beta_{C(II)}M_3 + \gamma_{C(II)}R \\ & \alpha_{A(III)}M_3 + A \Leftrightarrow \beta_{A(III)}M_4 + \gamma_{A(III)}Q & \alpha_{C(III)}M_3 + C \Leftrightarrow \beta_{C(III)}M_4 + \gamma_{C(III)}R \end{array} \quad \textbf{(3)}$$

The reaction kinetics for such interactions were formulated by Rahimi and Niksiar [40], extending the system originally proposed in Szekely [41]. Calculations from the procedures are based on the mentioned literature, with necessary adjustments to represent the proposed model.

The stoichiometric coefficient values, along with reaction parameters for each species are available in *Table 1*. The conversion of solids is a function of gas reaction rates (*Rj*), which are calculated using *equation 4*. These rates are evaluated over the available solid surface area and represented through relevant units (mol.cm^{-2}. s^{-1}) for any gas (*j*) reacting with a solid phase (*i*).

$$R_{j,i} = k_{j,i}\left(C_{A/C} - \frac{C_{Q/R}}{K_{eq.j,i}}\right) \quad \textbf{(4)}$$

Changes occur within the volume of the solid phase *M1* because of the shrinking radius. *Equation 5* describes the molar profile of the innermost solid core (Fe_2O_3) affected by parallel surface reactions.

$$\frac{d\left(\frac{4}{3}\pi {r_1}^3\right)}{dt}\rho_1 = -4\pi {r_1}^2\left[\alpha_{A(I)}R_{A(I)} + \alpha_{C(I)}R_{C(I)}\right] \quad \textbf{(5)}$$

where ρ refers to solid density in mol.cm^{-3}.

Evaluating the derivative of *equation 5*, the final expression for *M1* concentration is defined through its shrinking radius in *equation 6*.

$$\frac{dr_1}{dt} = -\frac{1}{\rho_1}\left[\alpha_{A(I)}R_{A(I)} + \alpha_{C(I)}R_{C(I)}\right] = -\frac{1}{\rho_1}\sum_{j=A,C}\alpha_j R_j \quad \textbf{(6)}$$

Solid phase *M2* is consecutively produced by the first reaction and consumed through the second during reactions. The effective volume of *M2* present in the grain is calculated through the remaining volume from the reduced core ($\frac{4}{3}\pi({r_2}^3 - {r_1}^3)$). Utilizing a similar derivative approach, molar profiles of each reactant phase M_i with $i > 1$ can be calculated through *equation 7*.

$$\frac{dr_i}{dt} = -\frac{1}{\rho_i}\sum_{j=A,C}\alpha_j R_j + \frac{r_{i-1}^2}{r_i^2}\left\{\frac{1}{\rho_i}\sum_{j=A,C}\beta_{j(i-1)}R_{j(i-1)} - \sum_{j=A,C,\cdots}^{m_i} - \frac{1}{\rho_{i-1}}\sum_{j=A,C}\alpha_{j(i-1)}R_{j(i-1)}\right\} \quad \textbf{(7)}$$

The MGM can be conveniently extended to incorporate any number of consecutive and parallel gas-solid reactions, proving beneficial for complex systems. The surface radii of solid phases represent their volume fractions, for determining the outlet pellet concentrations. Since grain operates at a relatively small scale, it is suitable to express the solid profiles as conversions ($0 < f_{Mi} < 1$) with *equation 8*.

$$f_{Mi} = 1 - \left(\frac{r_i}{r_g}\right)^3 \quad \textbf{(8)}$$

where r_g defines the grain outer radius.

Gaseous species in the current reduction process (gaseous reactants *A and C* in *equation 3*) offer separate parallel reactions to produce their respective products (*Q and R* in *equation 3*). This implies that the molar volumes of *A/Q* and *C/R* systems are conserved based on *P6*. Hence, it is assumed that the total gas concentration (C_t) remains unchanged during the process. The gas mass transfer can be described by a diffusive flux (N_j) due to the concentration difference between bulk and pellet phases. The values of N_j (mol.cm^{-2}. s^{-1}) can be computed using *equation 9*, where the gas is assumed to diffuse along the pellet radius (R_p) until the center.

$$N_j = -D_{ej}C_t\frac{y_{j,b} - y_{j,p}}{R_p} \quad \textbf{(9)}$$

The term $(y_{j,b} - y_{j,p})$ from the expression above computes the concentration difference between the bulk and pellet gas using the mol fractions. Parameter D_{ej} is known as the diffusion coefficient, and their values can be readily calculated through the existing correlations from the literature. The inward radial flow of gases can develop concentration profiles within the granular bed of the pellet. For the current analysis, the changes in the pellet are assumed to be negligible on a reactor scale, causing even distribution of diffused gas and grain conversions throughout the structure. Material balance for gas species is specified within *equation 10*.

$$\frac{\partial(\varepsilon_p C_t y_{j,p})}{\partial t} = \frac{N_j . A_p}{V_p} - \frac{3(1-\varepsilon_p)}{R_g^3}\sum_{i=1,2,3}\sum_{j=A,C} r_i^2 R_j \quad \textbf{(10)}$$

where ε_p, A_p and V_p denote the pellet porosity, surface area, and volume, respectively. The changes in gas concentration are expressed as mol fractions since the term $(\varepsilon_p C_t)$ on the left side of *equation 10* is constant. The computations represented in *equations 4-10* describe the reactions within a single pellet using MGM, serving as the foundation for developing reactor scale simulation.

3.2. Reactor-scale model

The pellet-scale profiles from the previous section can be integrated to approximate the behavior in a counter-current MBR. The dynamic behavior of the proposed isothermal reducer is constrained to the following assumptions.

T1. Plug flow of gases
T2. Isothermal operation
T3. No radial profiles due to the high L/D ratio of the reaction tube
T4. Solid downflow velocity (u_s) is negligible compared to gas (u_g)
T5. Pellet volume does not change during reactions.
T6. Constant bed porosity within the reaction tube

The behavior of a unit bed cross-section area in MBR is modelled using the profiles of a single pellet (*T3*). The mass flow rate (P_s) of the solid must be defined, for determining the number of pellets entering the system per unit of time ($\dot{n}_p$) in *equation 11*.

$$\dot{n}_p = \frac{P_s}{\frac{4}{3}\pi R_p^3 \rho_1 (1-\varepsilon_p) M_{ws}} \quad \textbf{(11)}$$

where MW_s denotes the molecular weight of inlet solid (Fe_2O_3) in g/mol. Since the volume of pellets is assumed constant (*T5*), the pellet flow is maintained at the reducer exit. The values of $\dot{n}_p$, along with the computed pellet concentration (*equation 8*) provides the flow rates for each solid species.

The gas entering the reaction tube diffuses into the bed of particles through the surface area (A_b), which is a function of the type of packing employed. In the current study, it is assumed that a random packing of the solid, in which the bed porosity (ε_b) is estimated with the available tube and pellet diameters (D_t and D_p respectively). The correlation for ε_b in a bed of closely packed solids is shown in *equation 12*.

$$\varepsilon_b = 0.39 + \frac{1.74}{(\frac{D_t}{D_p}+1.14)} \; ; \; 1.5 < \frac{D_t}{D_p} < 50 \quad \textbf{(12)}$$

The expression above is valid within the specified range, which describes the constraints over particle and reactor sizes. Gas generates concentration profiles along the axial reactor length (z), which are computed in the bulk phase according to *equation 13*.

$$\frac{\partial}{\partial z}\left(u_g c_t y_j\right) = -\left[\frac{A_p \dot{n}_p}{A_b u_s}\left(N_j - \sum_{j=1}^{k} R_j\right)\right] \quad \textbf{(13)}$$

The above-mentioned equation models the bulk phase gas interactions as a stationary FBR, which is valid under the conditions described in assumption *T4*. It is worth noting that the N_j is considered a positive value in *equation 10* as the gas enters the pellet through diffusion. Similarly, the flux is negative over the reactor scale (*equation 13*) due to the outflow of gas from the bulk phase.

3.3. System initialization

The system of partial differential equations (PDEs) in *sections 3* and *4* can be solved numerically through MATLAB software, providing interactive time-series responses. The initial operating conditions can be retrieved from the available literature, thus completing the dynamic model. The described MGM was verified by Rahimi and Niksiar [40] over the experiments conducted by Takenaka, Kimura [42] for the DRI process in an MBR. The model predicted the conversions based on varying flow rates and H_2/CO ratios in the syngas. High accuracies were recorded over multiple simulations, with a 1.2% average error for the entire investigation [40]. These findings suggest that MGM can produce reliable predictions for syngas reduction of iron-oxides in a moving bed. The set of operating conditions and design specifications obtained within literature exploring the CLHP process is illustrated in Table 2. Although a majority of the values are from Rahimi and Niksiar [40],

some key parameters have been updated based on literature recommendations over optimum CLHP operation. These conditions may exhibit deviations in performance from the DRI process, and justification is necessary to establish the reliability of results.

Table 2. The initial specification for reducer design.

Parameter (units)	Values	Reference
D_t (cm)	25	[40]
D_p (cm)	1.22	[40]
ε_p	0.22	[40]
Gas flow rate (cm^3/s)	28,666.67	[40]
P_s (g/s)	17.39	[40]
Mole ratio H_2/CO	2	[43]
T (K)	1,173	[44]
Pressure (atm)	20	[44]

Results were collected by solving the PDEs (*equations 6, 7, 10 and 13*) simultaneously using the MATLAB solver, capable of computing highly complex non-linear functions. The moving bed-type behavior was simulated as interconnected FBR units representing a small section of the reducer. Gas conversion at the top of the reducer is initially guessed for generating solid profiles, which serve as the input for the next part. The sections were repeatedly iterated by updating the initial guess with the generated values until the model converges, providing a solution for both exit gas and solid streams. The sections were added until the desired conversion was achieved, and the updated length provides the reaction tube dimensions for conducting process optimization. This method is also known as the finite difference scheme, a common approach for solving a complex system of numerous differential equations. The profiles generated on the reactor scale were analyzed to investigate dynamic behavior and improve conversions. Such an analysis is expected to provide scale-up criteria for designing a commercial CLHP reducer, which has not been investigated within the existing research. Thus, this study provides an essential contribution to the industrialization of this CLHP technology.

4. Results and discussions

The molar profiles of solid and gas reactants are exhibited in Fig. 4 and 5 as a function of bed length. Gas-side representations (mol. fractions) start from the bottom of the bed (Fig. 5), and solids (conversion) begin at the top (as shown in Fig. 4), illustrating their respective flows. Non-isothermal model verification devised by Rahimi and Niksiar [40] (as shown in Fig. 6) is presented for model verification, considering the majority of the system parameters (Table 2) are taken from the source.

4.1. Model verification

The current system reached equilibrium at length (L) of around 90 cm, though the reference case suggested completion at L = 200 cm. This observation can be justified through the isothermal system, indicating that T represents a strong relationship with reaction rates. Pellets within the reference case were assumed to enter the vessel at ambient conditions (T = 298 K) and contact with hot gas stream improves conversion along the bed length. This results in a significant drop in T (~500 K), causing retardation of the reaction. Previous investigations have highlighted similar observations, suggesting thermal control as a critical optimization approach for CLC-type processes [45, 46]. The solid formed reaction zones along the length for each oxidation state (Fe_2O_3: 0-30 cm, Fe_3O_4: 45-60 cm, FeO: 60-75 cm), with FeO as the major product (>99.9%) in the outlet. The reference case studied the DRI

process, where achieving the final OC state (Fe) was a critical target. Avoiding complete reduction of OC is preferable for CLHP, as it lowers the gas requirements in the reducer and oxidizer. Moreover, it was found that the presence of Fe can reduce the selectivity of syngas products in the reducer (CO_2 and H_2O) by more than 20%, leading to unconverted gas and inefficient CCS [24].

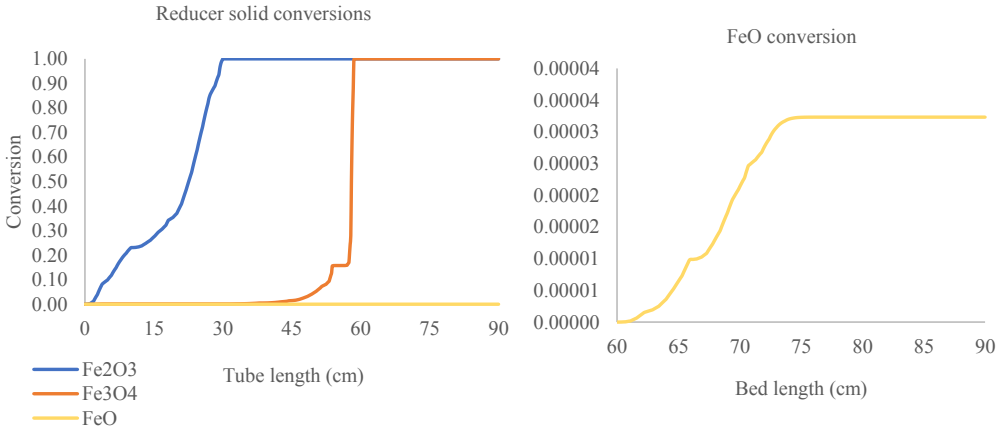

(a) (b)

Fig. 4. Solid conversion along tube length for (a) total system and (b) FeO

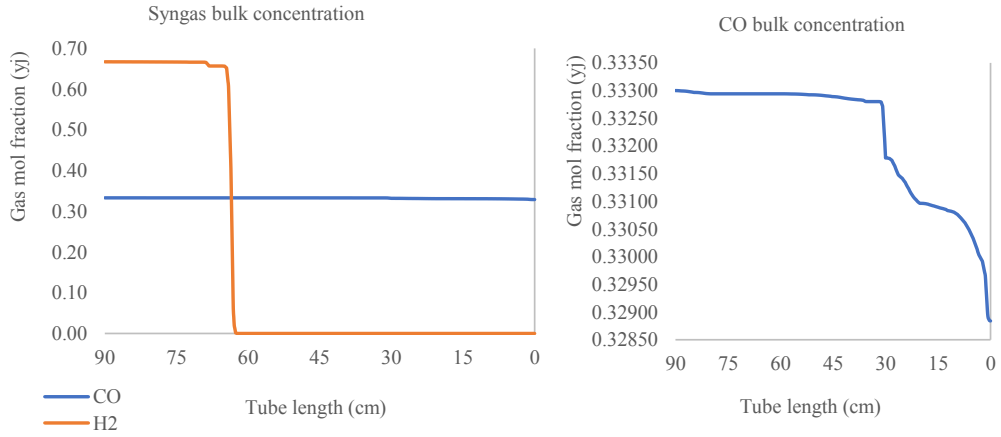

(a) (b)

Fig. 5. Gas concentration in bulk phase for (a) total syngas and (b) CO

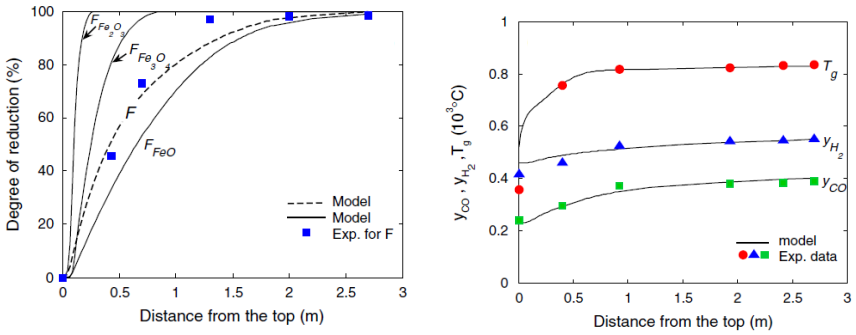

(a) (b)

Fig. 6. Reference case from Rahimi and Niksiar [40] representing (a) solid and (b) gas phases

Simulated gas conversions (as shown in Fig. 4) indicate rapid conversion of H_2 over a small effective length (60-70 cm), whereas the reaction zone for CO was relatively larger (~45 cm). The rates for H_2 reported in the literature are approximately 5 times the CO values, implying that the responses demonstrate expected behavior. Large amounts of H_2 could be oxidized through small amounts of FeO, and minute concentrations of CO proved sufficient to reducer both Fe_2O_3 and Fe_3O_4. These results can be validated through the equilibrium composition analysis, using the phase diagrams in Fig. 7. Fuel reduction selectivity favors H_2 (0.848) over CO (0.811), promoting its reactions initially at the bottom of the bed [24]. The H_2/ H_2O solid phase (Fig. 7 (b)) under the defined operation (T = 1173 K, y_j = 0.667) lies approximately at the FeO/Fe equilibrium line, which can confirm the presence of microscopic quantities of Fe. Although the diagram suggests small quantities of gas remaining at equilibrium, the complete conversion may be explained through the elevated pressure (20 atm) compared to the reference case (1 atm). High-pressure conditions promote gas conversion during the fuel reduction, allowing significant reduction of capital cost [47]. The phase for CO/ CO_2 equilibrium (Fig. 7 (a)) indicates FeO, which can explain the rapid reduction of both initial solid phases with minimal concentrations. It is worth noting that the literature results demonstrated a higher rate of CO in the syngas, likely due to the large temperature drop. These findings suggest that the syngas conversions may be improved by lowering system temperature, which may be vital for non-isothermal and temperature control investigations.

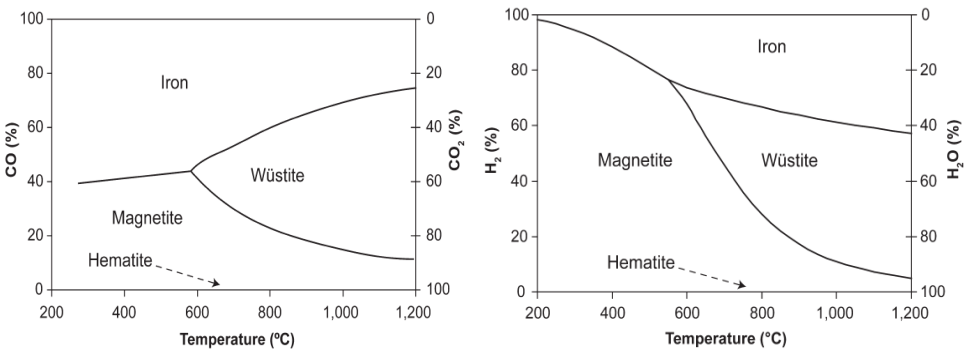

Fig. 7. Equilibrium phases of iron in (a) CO/CO_2 and (b) H_2/H_2O systems [48]

Profiles from the proposed dynamic model are thus in fair agreement with the available evidence in the literature. Hence, the developed simulation can be tested under varying conditions such as flow rates, temperature, pressure, and others for performance optimization.

4.2. Gas-solid ratio optimization

The operating conditions for the DRI process often aim toward complete solids reduction, which requires large amounts of gas. In the CLHP reducer, achieving complete syngas conversion is a crucial part of the CCS strategy. Since both gas and solid flow rates can be modified, conversion optimization is attempted through the gas-solid volumetric ratio (V_{gs}). The importance of this ratio in enhancing syngas profiles has been reported in previous simulation investigations [43, 49]. The V_{gs} values of the initially defined CLHP system were lowered by increasing the solid rate while simultaneously reducing gas flow. The outlet mol fraction of gas species in the reducer is illustrated as a function of V_{gs} in Fig. 8. Solid conversions remain unaffected during this investigation and are not displayed for clearer representation. The conversion of CO produced negligible effect over a large range of V_{gs}, suggesting that low gas flow rates might be necessary to achieve the desired conversion. However, after a value of around 682, the conversion rates improved significantly (marked in green in Fig. 8). The gas flow rate was then further reduced until 170, where outlet CO mol fraction 0.275 could be achieved. Solid velocity at this point (u_s = 0.197 cm/s) is approximately 1% of the gas flow (u_g = 20.382 cm/s), suggesting that assumption *T4* might not be valid after this range. Although there have been no studies investigating the negligibility criteria between gas-solid flows, we have assumed this value as the lower limit of gas flow rate (10,000 cm^3/s) at the specified solid flow (P_s = 240 g/s).

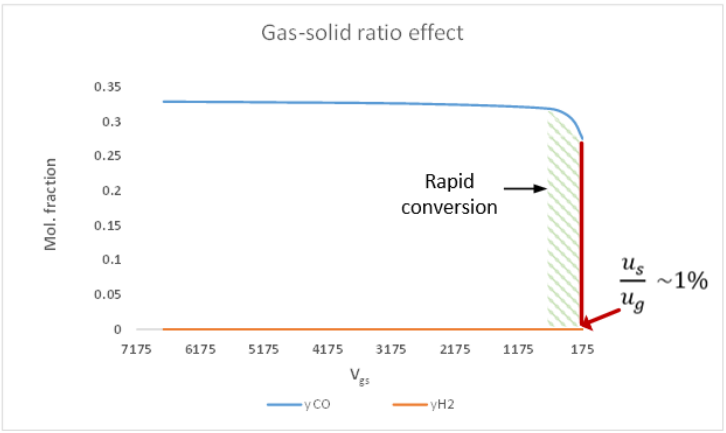

Fig. 8. Gas conversions for varying gas-solid ratio

Prior to scale-up design, the gas conversion must be improved to execute the efficient CCS system described for CLHP. Although complete conversion is the ideal target, National Physical Laboratory recommends 95% purity within conceptual designs [50]. Since gas flow rate analysis is limited through *T4*, other parameters affecting reaction rates must be considered for further optimization. CLHP reactions are highly sensitive to energy changes as CO oxidation is favored at a lower temperature, and H_2 reacts readily at elevated values [40]. These findings suggest that there may be a trade-off among H_2-CO conversions under isothermal operation and a drop in temperature may be necessary to achieve CCS requirements. Assessment of allowable limits requires non-isothermal modelling and optimization procedure, which can be implemented to extend the current design. The relevant computational procedures are available in the literature [41] and serve as essential prospects for future research. The pellet structure can also have a major impact on the reaction behavior, as smaller pellets offer a relatively even distribution of pores [51]. Reducing pellet size also lowers the

bed porosity (*equation 12*), which increases the reaction surface area available for gas. However, smaller pellets also suffer from a lower minimum fluidization velocity (u_{mf}), referring to the gas velocity (u_g) beyond which the bed starts experiencing high upwards thrust [52]. The fluidization condition can produce the bubbling behavior of the bed, which may cause particle attrition due to rapid movement [32]. MBRs are constrained to operate below u_{mf}, serving as an essential reactor design constraint. The final optimized reducer model can be scaled-up through the optimum V_{gs}, increasing gas flow in response to the added vessel length. Through this method, it can be ensured that commercial design does not operate near the minimum design limits ($u_s/ u_g \sim 1\%$), thus restricting the vessel length. Therefore, the significance of V_{gs} is justified for the process optimization and reactor design of CLHP. Although the calculated values for each study may differ in accordance with the design requirements, modelling procedures presented in this article serve as key information to implement isothermal reducer simulations. Furthermore, the identified process limitations and design criteria contribute towards the extension of the current analysis, ultimately aimed at commercial process design.

5. Conclusion

This paper has explored several aspects of the reducer as the most complex unit among the three CLHP process units. Despite its complexity, the reducer's reaction kinetics can fit into the MGM framework, describing complex multi-phase interactions between gas and solid. The pellet-scale model successfully enables the computation of the profiles in a countercurrent MBR tube. Note that the simulations of the developed models agree with the non-isothermal profiles reported in the literature. The simulation suggests that the temperature control can lead to a lower vessel length due to accelerated reaction rates observed in the solid phase. Additionally, the simulation shows that the elevated pressure assisted H_2 in achieving complete conversion, requiring complete conversion of CO as the optimization target.

Extra simulation on the reactor tube section attempts to explore the impact of varying V_{gs} values by increasing solid flow while simultaneously lowering the gas content. The results show that the effects are significant over a wide range of high V_{gs} values. It is worth noting that the gas conversion shows a significant improvement at a low V_{gs} value of about 682. The lower limit of this ratio (V_{gs} = 170) was defined based on the assumption T4, although the acceptable values to consider as negligibility remain unknown. Investigating the limits of T4 could help optimize gas conversions through flow rates, as the gas conversion appears to increase rapidly around the defined lower limit. For further study, it is crucial to investigate the effects of temperature and pellet size, which are vital to process optimization. A more detailed examination of an allowable temperature drop is also advisable for non-isothermal optimization, given that a favorable CO conversion occurs at lower values. It is also crucial to highlight the limitation on the vessel length in the MBR design constraints ($u_g < u_{mf}$), which may arise due to a pellet size reduction.

References

[1] Wang, Z., et al., Dynamic linkage among industrialisation, urbanisation, and CO2 emissions in APEC realms: Evidence based on DSUR estimation. Structural Change and Economic Dynamics, 2020. **52**: p. 382-389.

[2] Crabtree, G.W. and M.S. Dresselhaus, *The Hydrogen Fuel Alternative.* MRS Bulletin, 2008. **33**(4): p. 421-428.

[3] Lim, Z.-W. and K.-L. Goh, Natural gas industry transformation in Peninsular Malaysia: The journey towards a liberalised market. Energy Policy, 2019. **128**: p. 197-211.

[4] Zhao, H., *2022 Pioneers in Energy Research: Anders Lyngfelt.* Energy & Fuels, 2022. **36**(17): p. 9365-9370.

[5] Elmisaoui, S., et al., Shrinking Core Approach in the Modelling and Simulation of Phosphate Ore Acidulation. Chemical Engineering Transactions, 2021. **86**: p. 871-876.

[6] Monazam, E.R., R.W. Breault, and R. Siriwardane, *Kinetics of Magnetite (Fe3O4) Oxidation to*

Hematite (Fe2O3) in Air for Chemical Looping Combustion. Industrial & Engineering Chemistry Research, 2014: p. 13320-13328.
[7] Long, Y., et al., NiO and CuO coated monolithic oxygen carriers for chemical looping combustion of methane. Journal of the Energy Institute, 2021. **94**: p. 199-209.
[8] Kataria, P., J. Nandong, and W.S. Yeo. Reactor design and control aspects for Chemical Looping Hydrogen Production: A review. in 2022 International Conference on Green Energy, Computing and Sustainable Technology (GECOST). 2022. IEEE.
[9] Richter, H.J. and K.F. Knoche, *Reversibility of Combustion Processes*, in *Efficiency and Costing*. 1983, AMERICAN CHEMICAL SOCIETY. p. 71-85.
[10] Lyngfelt, A., et al., *11,000 h of chemical-looping combustion operation—Where are we and where do we want to go?* International Journal of Greenhouse Gas Control, 2019. **88**: p. 38-56.
[11] Abuelgasim, S., W. Wang, and A. Abdalazeez, A brief review for chemical looping combustion as a promising CO2 capture technology: Fundamentals and progress. Science of The Total Environment, 2021. **764**: p. 142892.
[12] Ayodele, B., et al., A Mini-Review on Hydrogen-Rich Syngas Production by Thermo-Catalytic and Bioconversion of Biomass and Its Environmental Implications. Frontiers in Energy Research, 2019. **7**.
[13] Łukajtis, R., et al., *Hydrogen production from biomass using dark fermentation.* Renewable and Sustainable Energy Reviews, 2018. **91**: p. 665-694.
[14] Cao, L., et al., Biorenewable hydrogen production through biomass gasification: A review and future prospects. Environmental research, 2020. **186**: p. 109547.
[15] Baykara, S.Z., Hydrogen production by direct solar thermal decomposition of water, possibilities for improvement of process efficiency. International Journal of Hydrogen Energy, 2004. **29**(14): p. 1451-1458.
[16] Dincer, I., *Green methods for hydrogen production.* International Journal of Hydrogen Energy, 2012. **37**(2): p. 1954-1971.
[17] Winkler, H., et al., *Access and Affordability of Electricity in Developing Countries.* World Development, 2011. **39**(6): p. 1037-1050.
[18] Chiesa, P., et al., *Three-reactors chemical looping process for hydrogen production.* International Journal of Hydrogen Energy, 2008. **33**(9): p. 2233-2245.
[19] Yan, X., et al., Performance of hydrogen and power co-generation system based on chemical looping hydrogen generation of coal. International Journal of Hydrogen Energy, 2022.
[20] Feng, Y., N. Wang, and X. Guo, Reaction mechanism of methane conversion over Ca2Fe2O5 oxygen carrier in chemical looping hydrogen production. Fuel, 2021. **290**: p. 120094.
[21] Condori, O., et al., Biomass chemical looping gasification for syngas production using ilmenite as oxygen carrier in a 1.5 kWth unit. Chemical Engineering Journal, 2021. **405**: p. 126679.
[22] Condori, O., et al., Biomass chemical looping gasification for syngas production using LD Slag as oxygen carrier in a 1.5 kWth unit. Fuel Processing Technology, 2021. **222**: p. 106963.
[23] Yan, J., et al., Hydrogen-rich syngas production with tar elimination via biomass chemical looping gasification (BCLG) using BaFe2O4/Al2O3 as oxygen carrier. Chemical Engineering Journal, 2020. **387**: p. 124107.
[24] Kang, K.-S., et al., Oxygen-carrier selection and thermal analysis of the chemical-looping process for hydrogen production. International Journal of Hydrogen Energy, 2010. **35**(22): p. 12246-12254.
[25] Ma, S., et al., Enhanced performance of hematite oxygen carrier by CeO2 for chemical looping hydrogen generation. 2022. **47**(8): p. 5130-5141.
[26] Kathe, M., et al., Chemical looping gasification for hydrogen enhanced syngas production with in-situ CO2 capture. 2014, The Ohio State Univ., Columbus, OH (United States).
[27] Dou, B., et al., Renewable hydrogen production from chemical looping steam reforming of biodiesel byproduct glycerol by mesoporous oxygen carriers. Chemical Engineering Journal, 2021. **416**: p. 127612.

[28] Zhou, Q., L. Zeng, and L.-S. Fan Syngas Chemical Looping Process: Dynamic Modeling of a Moving-Bed Reducer. Research Gate, 2013.
[29] Kooiman, R.F., et al., Experimental Demonstration of Two-Stage Packed Bed Chemical-Looping Combustion Using Syngas with CuO/Al2O3 and NiO/CaAl2O4 as Oxygen Carriers. Industrial & Engineering Chemistry Research, 2015. **54**(7): p. 2001-2011.
[30] Diglio, G., et al., Sensitivity analysis in the design of a packed-bed reactor for a chemical looping combustion process. 2017.
[31] Zerobin, F. and T. Pröll, *Potential and limitations of power generation via chemical looping combustion of gaseous fuels.* International Journal of Greenhouse Gas Control, 2017. **64**: p. 174-182.
[32] Zhou, Z., L. Han, and G.M. Bollas, Overview of chemical-looping reduction in fixed bed and fluidized bed reactors focused on oxygen carrier utilization and reactor efficiency. Aerosol and Air Quality Research, 2014. **14**(2): p. 559-571.
[33] Dou, B., et al., Hydrogen production by enhanced-sorption chemical looping steam reforming of glycerol in moving-bed reactors. Applied Energy, 2014. **130**: p. 342-349.
[34] Tong, A., et al., Continuous high purity hydrogen generation from a syngas chemical looping 25kWth sub-pilot unit with 100% carbon capture. Fuel, 2013. **103**: p. 495-505.
[35] Zhu, J., et al., Modeling and design of a multi-tubular packed-bed reactor for methanol steam reforming over a Cu/ZnO/Al2O3 catalyst. Energies, 2020. **13**(3): p. 610.
[36] OYEGOKE, T., et al., Design and Fabrication of a Multi-tubular Fixed Bed Reactor for Acetone Production as A Pilot Plant Model for Chemical Engineering Training in Developing Nations. Journal of the Pakistan Institute of Chemical Engineers, 2022. **50**(2).
[37] Pelaez, R., et al., Direct synthesis of dimethyl ether in multi-tubular fixed-bed reactors: 2D multi-scale modelling and optimum design. Fuel Processing Technology, 2018. **174**: p. 149-157.
[38] Rahimi, A. and A. Niksiar, A general model for moving-bed reactors with multiple chemical reactions, Part II: Effect of kinetic model. International Journal of Mineral Processing, 2013. **124**: p. 67-74.
[39] Tonks, M.R., P.-C.A. Simon, and J. Hirschhorn, *Mechanistic grain growth model for fresh and irradiated UO2 nuclear fuel.* Journal of Nuclear Materials, 2021. **543**: p. 152576.
[40] Rahimi, A. and A. Niksiar, A general model for moving-bed reactors with multiple chemical reactions part I: Model formulation. International Journal of Mineral Processing, 2013. **124**: p. 58-66.
[41] Szekely, J., *Gas-solid reactions*. 2012: Elsevier.
[42] Takenaka, Y., et al., Mathematical model of direct reduction shaft furnace and its application to actual operations of a model plant. Computers & chemical engineering, 1986. **10**(1): p. 67-75.
[43] Kuo, P.-C., et al., Hydrogen production from biomass using iron-based chemical looping technology: Validation, optimization, and efficiency. Chemical Engineering Journal, 2018. **337**: p. 405-415.
[44] Cleeton, J.P.E., et al., Clean hydrogen production and electricity from coal via chemical looping: Identifying a suitable operating regime. International Journal of Hydrogen Energy, 2009. **34**(1): p. 1-12.
[45] Song, Q., et al., Effect of temperature on reduction of CaSO4 oxygen carrier in chemical-looping combustion of simulated coal gas in a fluidized bed reactor. Industrial & Engineering Chemistry Research, 2008. **47**(21): p. 8148-8159.
[46] Ryu, H.-J., D.-H. Bae, and G.-T. Jin, Effect of temperature on reduction reactivity of oxygen carrier particles in a fixed bed chemical-looping combustor. Korean Journal of Chemical Engineering, 2003. **20**: p. 960-966.
[47] Sandvik, P., et al., *Operating Strategy of Chemical Looping Systems with Varied Reducer and Combustor Pressures.* Industrial & Engineering Chemistry Research, 2019. **58**(13): p. 5228-5235.

[48] Zhang, X. and H. Jin, Thermodynamic analysis of chemical-looping hydrogen generation. Applied Energy, 2013. **112**: p. 800-807.
[49] Li, F., et al., Syngas chemical looping gasification process: Bench-scale studies and reactor simulations. AIChE Journal, 2010. **56**(8): p. 2186-2199.
[50] *Copyright*, in *Strategies of Banks and Other Financial Institutions*, R. Kumar, Editor. 2014, Academic Press: San Diego. p. iv.
[51] Dwarapudi, S., et al., Influence of pellet size on quality and microstructure of iron ore pellets. ISIJ international, 2008. **48**(6): p. 768-776.
[52] Cocco, R., S.R. Karri, and T. Knowlton, *Introduction to fluidization.* Chem. Eng. Prog, 2014. **110**(11): p. 21-29.